# University of Groningen

## Single-Source, Solvent-Free, Room Temperature Deposition of Black γ-CsSnI3 Films

Kiyek, Vivien M.; Birkhölzer, Yorick A.; Smirnov, Yury; Ledinsky, Martin; Remes, Zdenek; Momand, Jamo; Kooi, Bart J.; Koster, Gertjan; Rijnders, Guus; Morales-Masis, Monica

**IMPORTANT NOTE: You are advised to consult the publisher's version (publisher's PDF) if you wish to cite from it. Please check the document version below.**

*Document Version*
Publisher's PDF, also known as Version of record

[Link to publication in University of Groningen/UMCG research database](#)

# Single-Source, Solvent-Free, Room Temperature Deposition of Black γ-CsSnI₃ Films

*Vivien M. Kiyek, Yorick A. Birkhölzer, Yury Smirnov, Martin Ledinsky, Zdenek Remes, Jamo Momand, Bart J. Kooi, Gertjan Koster, Guus Rijnders, and Monica Morales-Masis**

The presence of a nonoptically active polymorph (yellow-phase) competing with the optically active polymorph (black γ-phase) at room temperature in cesium tin iodide (CsSnI₃) and the susceptibility of Sn to oxidation represent two of the biggest obstacles for the exploitation of CsSnI₃ in optoelectronic devices. Here room-temperature single-source in vacuum deposition of smooth black γ–CsSnI₃ thin films is reported. This is done by fabricating a solid target by completely solvent-free mixing of CsI and SnI₂ powders and isostatic pressing. By controlled laser ablation of the solid target on an arbitrary substrate at room temperature, the formation of CsSnI₃ thin films with optimal optical properties is demonstrated. The films present a bandgap of 1.32 eV, a sharp absorption edge, and near-infrared photoluminescence emission. These properties and X-ray diffraction of the thin films confirm the formation of the orthorhombic (B-γ) perovskite phase. The thermal stability of the phase is ensured by applying in situ an Al₂O₃ capping layer. This work demonstrates the potential of pulsed laser deposition as a volatility-insensitive single-source growth technique of halide perovskites and represents a critical step forward in the development and future scalability of inorganic lead-free halide perovskites.

Pulsed laser deposition (PLD) has offered unique options for the development of complex materials thin film growth, allowing stoichiometric transfer and multicompound deposition

independent of the relative volatility of the elements and ultimate control of interfaces. In the field of complex oxides, PLD opened the way to high-$T_c$ superconducting films requiring stoichiometric transfer of multiple (4–5) cations.[1] Here we present the rather unexplored but enormous potential of PLD as a unique single-source in-vacuum deposition technique of all-inorganic halide perovskites, using cesium tin iodide (CsSnI₃) as case example.

CsSnI₃ has been widely proposed in literature as a Pb-free and all-inorganic alternative to the archetypical hybrid halide solar cell absorber, CH₃NH₃PbI₃ (MAPbI₃). The replacement of toxic Pb with Sn is a natural choice due to their similar ionic radius and lower toxicity of Sn.[2] The replacement of the organic cation (e.g., CH₃NH₃) with Cs has been proposed to enhance the thermal stability of the material.[3] While the decomposition temperature of Cs-based halide perovskites is higher than the ones containing organic cations, the size of the Cs⁺ cation is at the limit for stability of the perovskite structure, and therefore causing phase instabilities[4–6] between the optically active (black) perovskite phase and the nonoptically active (yellow) nonperovskite phase. In CsSnI₃ these phases can coexist at room temperature. Black phase stabilization in all-inorganic perovskites is therefore critical to ensure their application in optoelectronic devices and has been the subject of very recent work, focused on CsPbI₃[7,8] and CsSnI₃.[9]

In terms of synthesis, solution-based processes are the most widely used techniques to fabricate these materials.[10–14] Concerns about the use of highly toxic solvents and complex device integration have recently motivated the investigation of solvent-free and vacuum-based thin film deposition processes.[11,15,16] Thermal coevaporation has been the main in-vacuum technique that enabled high quality thin film formation of a family of halide perovskites and high-efficiency devices.[11,17,18] However, the need for multiple sources due to the different volatility of the constituent elements poses a limitation for the synthesis of multication-multihalide materials and their further upscaling. Steps toward achieving a single-source deposition have sporadically been reported for laser-based techniques. This includes resonant infrared matrix assisted pulsed laser evaporation[19,20] and pulsed-laser deposition (PLD)[21–23] of MAPbI₃ and CsPbBr₃, but high material quality remains yet to

V. M. Kiyek, Y. A. Birkhölzer, Y. Smirnov, Prof. G. Koster, Prof. G. Rijnders, Dr. M. Morales-Masis
MESA+ Institute for Nanotechnology
University of Twente
P.O. Box 217, Enschede 7500 AE, The Netherlands
E-mail: m.moralesmasis@utwente.nl

Dr. M. Ledinsky, Dr. Z. Remes
Institute of Physics
Academy of Sciences of the Czech Republic
Cukrovarnická 10, Prague 162 00, Czech Republic

Dr. J. Momand, Prof. B. J. Kooi
Zernike Institute for Advanced Materials
University of Groningen
Nijenborgh 4, Groningen 9747 AG, The Netherlands

(iD) The ORCID identification number(s) for the author(s) of this article can be found under https://doi.org/10.1002/admi.202000162.
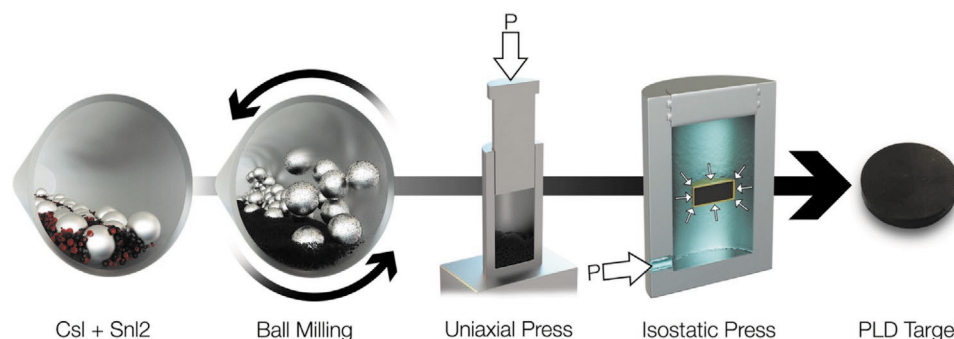
**Figure 1.** Illustration of PLD target fabrication process. From left to right: Stoichiometric mixture of CsI and SnI$_2$ powders, ball milling, uniaxial press applying 33 MPa and hydraulic press applying 360 MPa isostatically, and final target.

be demonstrated. An approach gaining popularity is the mechanochemical synthesis of halide perovskite powders and subsequent thin film formation following single-source vapor deposition (SSVD) of those powders.[24–26] However, SSVD might present hurdles on the exploration of a plethora of multication-multihalides and double-perovskites due to differing volatilities, i.e., off-stoichiometric transfer and/or sticking.

Here we present single-source room temperature PLD of CsSnI$_3$ thin films with excellent optical properties achieved by the formation of the orthorhombic black (B-$\gamma$) perovskite phase. This work introduces PLD as an enabling technology to achieve near-stoichiometric transfer of all-inorganic halide perovskites in vacuum, opening the path for controlled and reproducible growth as well as ease of integration in devices from photovoltaics to more complex architectures such as integrated photonics.

**Figure 1** summarizes the fabrication process of the solid PLD target. Equimolar amounts of CsI and SnI$_2$ source powders were mixed by ball-milling in an Ar-filled vessel. We note that the mixing is done only by rotation of the cylindrical vessel containing the powder and ZrO$_2$ balls, and therefore is different from the known mechanochemical synthesis.[26] To ensure a uniform mixture of the powders, the mixing process was left running for 3 d. The enhanced uniformity of the Cs, Sn, and I elemental distribution on the target with increasing mixing time was confirmed by energy-dispersive X-ray spectroscopy (Figure S1 and Table S1, Supporting Information). The mixed powders were then pressed into a 2 cm diameter disk-shaped pellet using a uniaxial press and subsequently exposed to an isostatic pressure of 360 MPa using a hydraulic press. A similar procedure has been used for the fabrication of Cs$_2$AgBiBr$_6$ wafers.[27] The isostatic pressing allows for the formation of a compact and dense target (>85% calculated density) as required for PLD. Therefore, no further sintering with heating was required. It is important to note that the pressed solid target does not react into the CsSnI$_3$ phase, as shown by the X-ray diffraction (XRD) pattern in Figure 3a.

The target was loaded into the PLD chamber, which was then evacuated to a base pressure of $\approx$1 $\times$ 10$^{-7}$ mbar. CsSnI$_3$ thin films were deposited onto Si (with native SiO$_x$), fused silica, and glass substrates at room temperature using a KrF (248 nm) laser and a fluence of 0.2 J cm$^{-2}$. The growth rate was 0.05 nm per pulse such that for a laser repetition frequency of 5 Hz, the total duration to grow 100 (200) nm CsSnI$_3$ was only 400 (800) s. An Ar working pressure of 1.3 $\times$ 10$^{-3}$ mbar was kept constant during deposition and no additional reactive gasses
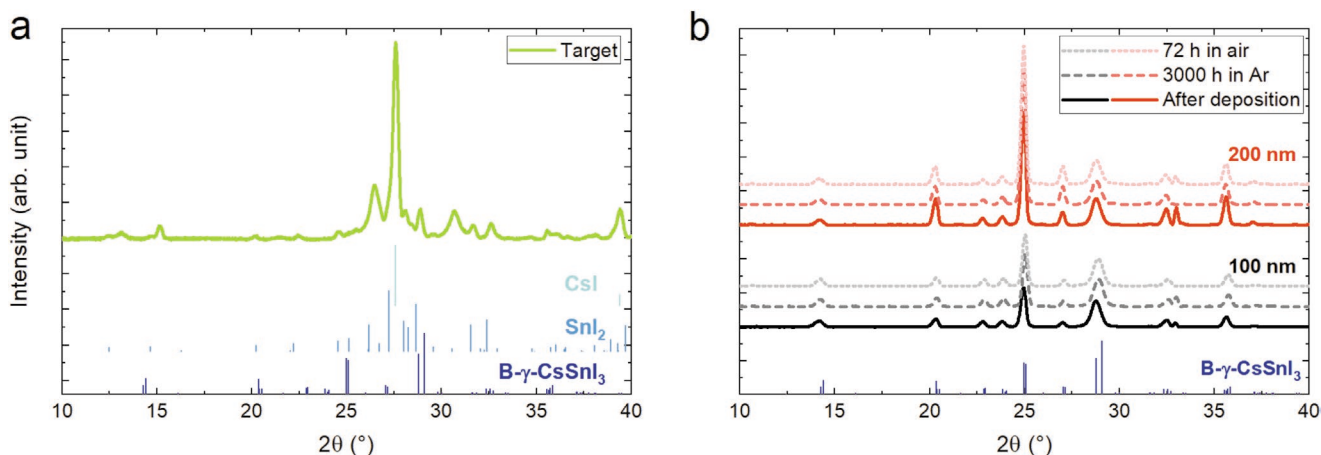
were introduced. Following CsSnI$_3$ deposition, an amorphous Al$_2$O$_3$ capping layer was applied in situ by PLD.

Steady-state photoluminescence (PL) spectra and absorption coefficient measurements were performed on 100 nm thick PLD-grown CsSnI$_3$ films on fused silica substrates (**Figure 2**). The PL emission is centered at 1.38 eV (900 nm). Consistently, the absorption coefficient determined by photothermal deflection spectroscopy (PDS) shows a sharp absorption edge centered at 1.32 eV. The absorption coefficient is shown with a solid black line and for comparison, the absorption coefficient (also determined by PDS) of a reference methylammonium lead halide (MAPbI$_3$) perovskite film[28] is shown with a dashed black line. These results highlight the high absorption coefficient at the whole visible spectral range and sharp edge, indicating a high quality absorber material, comparable to MAPbI$_3$.[28] In order to extract the Urbach energy, the absorption spectrum was calculated from the PL spectrum at the band edge area via the reciprocal relation.[29] Individually, this recalculated absorption spectra and the absorption coefficient measured by PDS both confirm an Urbach energy of 12.9 meV for the PLD grown CsSnI$_3$ films. This is only 0.4 meV higher that of MAPbI$_3$ (12.5 meV) determined by the same methods. Such a low Urbach energy indicates potential for low voltage losses in the optimized solar cell.[30]

A bandgap of 1.32 eV extracted from the Tauc plot (Figure S3, Supporting Information) and the aforementioned optical
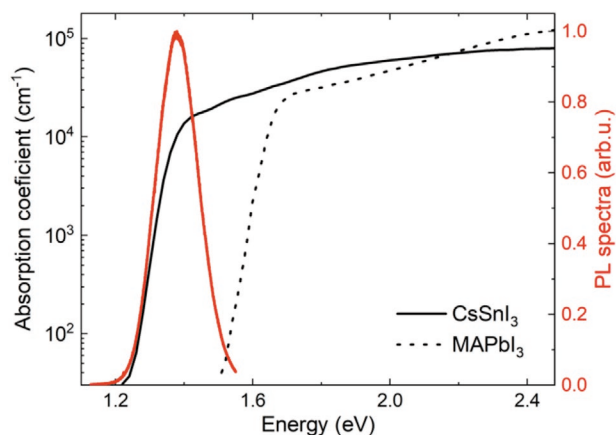


**Figure 2.** Absorption coefficient (left axis) and steady state PL (right axis) of 100 nm CsSnI$_3$ PLD grown films. To highlight the sharp absorption edge of the CsSnI$_3$, the absorption coefficient of a reference MAPbI$_3$ film is presented.

**ADVANCED
SCIENCE NEWS**

www.advancedsciencenews.com

**ADVANCED
MATERIALS
INTERFACES**

www.advmatinterfaces.de

**Figure 3.** a) X-ray diffraction (XRD) pattern of the solid PLD target shown in Figure 1. b) XRD patterns of 100 and 200 nm thick $CsSnI_3$ films deposited at room temperature by PLD. The solid lines are measurements directly after the deposition, the dashed lines after 3000 h in Ar atmosphere, and the dotted lines after additional 72 h in air. For comparison, the same B-$\gamma$-$CsSnI_3$ reference spectrum is plotted below in both graphs. The plots indicate that while the source target does not present the $CsSnI_3$ phase but a mixture of the CsI and $SnI_2$ powders, the resulting thin films present the single black orthorhombic phase of $CsSnI_3$, which is stable over long time thanks to the $Al_2O_3$ capping layer.

properties are characteristics of the black orthorhombic phase of $CsSnI_3$ (B-$\gamma$-$CsSnI_3$).[9] The formation of polycrystalline B-$\gamma$-$CsSnI_3$ thin films is confirmed by XRD. **Figure 3** displays the XRD patterns of the target and the thin films shown in this paper. Panel (a) indicates that the target is an unreacted mixture of CsI and $SnI_2$ powders, whereas panel (b) demonstrates that thin films grown from this target by PLD at room temperature crystallize in the perovskite structure and very well match the reference pattern of B-$\gamma$-$CsSnI_3$ following reference.[9] No difference between thin (100 nm) and thicker films (200 nm) was noticed, indicating that the B-$\gamma$-$CsSnI_3$ phase remains stable with doubled thickness (solid lines in Figure 3b). The dashed lines in Figure 3b are measurements taken four months ($\approx$3000 h) after fabrication of the films, where the films were stored in a glove box filled with argon gas, demonstrating that

the B-$\gamma$-$CsSnI_3$ phase of both film thicknesses remains stable even months after thin film fabrication. After these XRD measurements the same films were kept in open air for 72 h, measured again, and still showed no structural changes (dotted lines in Figure 3b). The $Al_2O_3$ capping layer with a thickness of 13 and 40 nm for the 100 and 200 nm thick $CsSnI_3$ films, respectively, is amorphous and therefore not present in the XRD spectra. Information about thin films grown from targets with different mixing times is found in Figure S2 in the Supporting Information.

Scanning transmission electron microscopy (STEM) results (**Figure 4**) confirm uniform sticking of the ablated elements and the formation of a smooth and dense film with large elongated grains along the thickness of the film (Figure 4a). Zoomed-in area of Figure 4a with enhanced contrast is shown in Figure S5
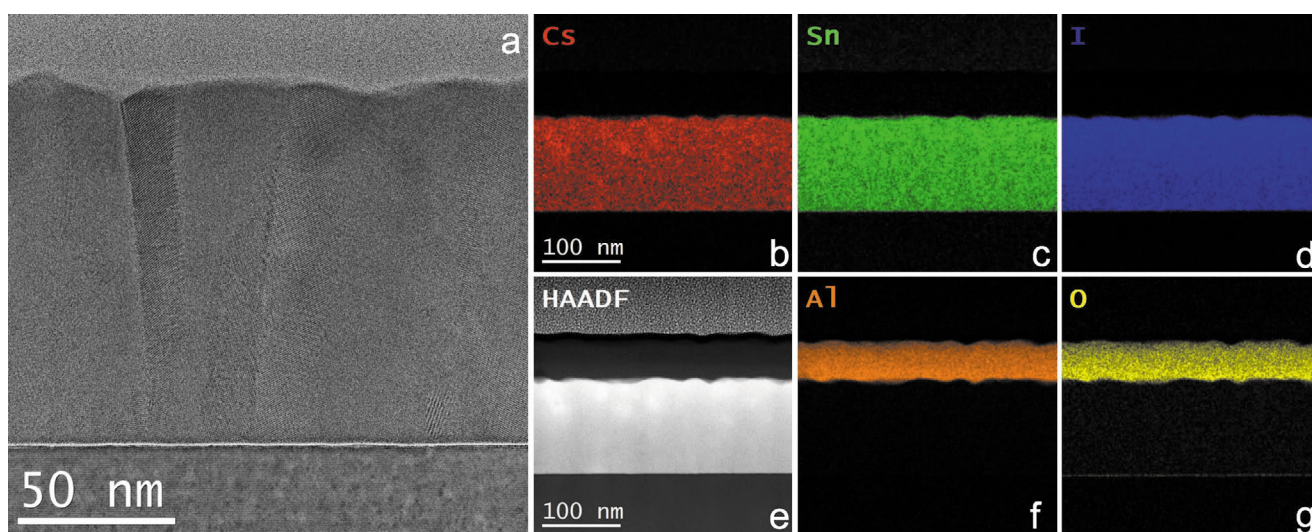


**Figure 4.** a) Cross-section bright-field TEM image of a PLD-grown B-$\gamma$-$CsSnI_3$ film on Si. The image shows the formation of a dense film with elongated crystalline grains. b–g) High-angle annular dark-field (HAADF) image and EDX mapping of the constituent elements of $CsSnI_3$ and the $Al_2O_3$ capping layer. EDX confirms uniform distribution of Cs, Sn, and I along the thickness of the layer and conformal coating of the $Al_2O_3$ capping layer.

**ADVANCED
SCIENCE NEWS**

www.advancedsciencenews.com

**ADVANCED
MATERIALS
INTERFACES**

www.advmatinterfaces.de

in the Supporting Information. The distribution of cesium (Cs), tin (Sn), and iodide (I) in the films was evaluated by cross-section energy-dispersive X-ray spectroscopy (EDX) mapping (Figure 4b–d). The EDX maps show a uniform distribution of the three elements across the thickness of the film and quantitative analysis indicate an overall Cs/Sn ratio of 1. Combining Rutherford back scattering (RBS) and particle induced X-ray emission (PIXE), we determined an iodide content in the films of ≈65 at% (Figure S4, Supporting Information). Figure 4f,g also shows conformal coating and uniformity of the amorphous $Al_2O_3$ protective layer. The low roughness of the $CsSnI_3$ + capped $Al_2O_3$ films was furthermore confirmed by atomic force microscopy (Figure S6, Supporting Information).

Concluding, we have demonstrated the feasibility of single-source in-vacuum deposition of B-$\gamma$–$CsSnI_3$ films by PLD. The high optical quality of the films and black phase confirmation by optical and structural characterization shows the enormous potential of PLD for the single source growth of halide perovskites even at room temperature. In comparison with recently reported SSVD, PLD presents the advantage of nonequilibrium ablation of a solid target, therefore allowing near-stoichiometric transfer insensitive to the different volatilities of the elements. Another demonstrated advantage of PLD is the possibility of depositing multilayers without breaking vacuum, in this case the application of the $Al_2O_3$ layer allowing the stabilization of the black phase and protection against oxidation. This work motivates further exploration of the electrical properties of the material as well as its integration in complex devices, such as absorbers in solar cell devices, monolithic tandem solar cells or efficient light emitters in integrated photonic circuits.

## Experimental Section

*Target Source Materials*: CsI and $SnI_2$ source powders were purchased from Sigma-Aldrich (99.9% purity) and TCI (>97.0% purity). For the $Al_2O_3$ deposition, an $Al_2O_3$ single crystal with rough surfaces to enhance laser absorption was used as source target.

*PLD*: The vacuum chamber was evacuated to a base pressure of ≈1 × $10^{-7}$ mbar. A KrF (248 nm) laser was used to ablate the fabricated $CsSnI_3$ target. Thin films were deposited onto Si (with native $SiO_x$), fused silica, and glass substrates at room temperature. An Ar working pressure of 1.3 × $10^{-3}$ mbar was kept constant during deposition and no additional reactive gasses were introduced. The laser frequency was kept at 5 Hz, target-to-substrate distance at 50 mm, and a fluence of 0.2 J $cm^{-2}$ was used. The deposition of the $Al_2O_3$ capping layer was performed under Ar atmosphere and room temperature as the $CsSnI_3$ film. $Al_2O_3$ is a large bandgap material (≈7 eV) with insignificant absorption in the measured spectral region, therefore, the measured optical properties are unaffected by the $Al_2O_3$ thin film.

*PDS*: Photothermal deflection spectroscopy directly measures the optical absorption of thin films with sensitivity of up to four orders of magnitude. The light absorption is determined via a sample heating effect, by measuring the deflection of a probe laser beam with a position-sensitive detector. The PDS spectrophotometer uses a 150 W Xe lamp as a light source and a monochromator equipped with grating blazed at 750 nm operating in a broad spectral range from ultraviolet to infrared region 400–1200 nm.

*PL*: Photoluminescence spectra are measured using an excitation laser at 442 nm in a Renishaw in-Via REFLEX spectroscope. The intensity of the excitation light is reduced in order to prevent any structural degradation during measurements.

*XRD*: The films were analyzed by X-ray diffraction, using a Bruker D8 Discover diffractometer with a high brilliance microfocus Cu rotating anode generator, Montel optics, a 1 mm pinhole beam collimator, and an EIGER2 R 500 K area detector.

*TEM*: Cross-sectional specimen were prepared with an FEI Helios G4 CX focused ion beam, using gradually decreasing acceleration voltages of 30, 5, and 2 kV. TEM analyses were performed with a double aberration corrected FEI Themis Z, operated at 300 kV. High-angle annular dark-field (HAADF)-STEM images were recorded with a probe currents between 50 and 200 pA, convergence semi-angle 21 mrad and HAADF collection angles 61–200 mrad. EDX spectrum imaging was performed with a probe current of 1 nA, where the spectra were recorded with a Dual-X system, providing in total 1.76 sr EDX detectors.

## Supporting Information

Supporting Information is available from the Wiley Online Library or from the author.

## Conflict of Interest

The authors declare no conflict of interest.

[1] D. Dijkkamp, T. Venkatesan, X. D. Wu, S. A. Shaheen, N. Jisrawi, Y. H. Min-Lee, W. L. McLean, M. Croft, *Appl. Phys. Lett.* **1987**, *51*, 619.

[2] G. Nasti, A. Abate, *Adv. Energy Mater.* **2020**, *10*, 1902467.

[3] M. Kulbak, D. Cahen, G. Hodes, *J. Phys. Chem. Lett.* **2015**, *6*, 2452.

[4] W. Travis, E. N. K. Glover, H. Bronstein, D. O. Scanlon, R. G. Palgrave, *Chem. Sci.* **2016**, *7*, 4548.

[5] S. Tao, I. Schmidt, G. Brocks, J. Jiang, I. Tranca, K. Meerholz, S. Olthof, *Nat. Commun.* **2019**, *10*, 2560.

[6] E. L. da Silva, J. M. Skelton, S. C. Parker, A. Walsh, *Phys. Rev. B* **2015**, *91*, 144107.

[7] J. A. Steele, H. Jin, I. Dovgaliuk, R. F. Berger, T. Braeckevelt, H. Yuan, C. Martin, E. Solano, K. Lejaeghere, S. M. J. Rogge, C. Notebaert, W. Vandezande, K. P. F. Janssen, B. Goderis, E. Debroye, Y. K. Wang, Y. Dong, D. Ma, M. Saidaminov, H. Tan, Z. Lu,

**ADVANCED
SCIENCE NEWS**

www.advancedsciencenews.com

**ADVANCED
MATERIALS
INTERFACES**

www.advmatinterfaces.de

V. Dyadkin, D. Chernyshov, V. Van Speybroeck, E. H. Sargent, J. Hofkens, M. B. J. Roeffaers, *Science* **2019**, *365*, 679.

[8] D. B. Straus, S. Guo, R. J. Cava, *J. Am. Chem. Soc.* **2019**, *141*, 11435.

[9] I. Chung, J.-H. Song, J. Im, J. Androulakis, C. D. Malliakas, H. Li, A. J. Freeman, J. T. Kenney, M. G. Kanatzidis, *J. Am. Chem. Soc.* **2012**, *134*, 8579.

[10] L. Protesescu, S. Yakunin, M. I. Bodnarchuk, F. Krieg, R. Caputo, C. H. Hendon, R. X. Yang, A. Walsh, M. V. Kovalenko, *Nano Lett.* **2015**, *15*, 3692.

[11] W. A. Dunlap-Shohl, Y. Zhou, N. P. Padture, D. B. Mitzi, *Chem. Rev.* **2019**, *119*, 3193.

[12] Q. Tai, K.-C. Tang, F. Yan, *Energy Environ. Sci.* **2019**, *12*, 2375.

[13] F. Liu, C. Ding, Y. Zhang, T. S. Ripolles, T. Kamisaka, T. Toyoda, S. Hayase, T. Minemoto, K. Yoshino, S. Dai, M. Yanagida, H. Noguchi, Q. She, *J. Am. Chem. Soc.* **2017**, *139*, 16708.

[14] J.-P. Correa-Baena, M. Saliba, T. Buonassisi, M. Grätzel, A. Abate, W. Tress, A. Hagfeldt, *Science* **2017**, *358*, 739.

[15] M. Chen, M.-G. Ju, H. F. Garces, A. D. Carl, L. K. Ono, Z. Hawash, Y. Zhang, T. Shen, Y. Qi, R. L. Grimm, D. Pacifici, X. C. Zeng, Y. Zhou, N. P. Padture, *Nat. Commun.* **2019**, *10*, 16.

[16] Z. Hong, D. Tan, R. A. John, Y. K. E. Tay, Y. K. T. Ho, X. Zhao, T. C. Sum, N. Mathews, F. García, H. S. Soo, *iScience* **2019**, *16*, 312.

[17] J. Ávila, C. Momblona, P. P. Boix, M. Sessolo, H. J. Bolink, *Joule* **2017**, *1*, 431.

[18] Z. Li, T. R. Klein, D. H. Kim, M. Yang, J. J. Berry, M. F. A. M. van Hest, K. Zhu, *Nat. Rev. Mater.* **2018**, *3*, 18017.

[19] E. T. Barraza, W. A. Dunlap-Shohl, D. B. Mitzi, A. D. Stiff-Roberts, *J. Electron. Mater.* **2018**, *47*, 917.

[20] W. A. Dunlap-Shohl, E. T. Barraza, A. Barrette, K. Gundogdu, A. D. Stiff-Roberts, D. B. Mitzi, *ACS Energy Lett.* **2018**, *3*, 270.

[21] U. Bansode, R. Naphade, O. Game, S. Agarkar, S. Ogale, *J. Phys. Chem. C* **2015**, *119*, 9177.

[22] Y. Huang, L. Zhang, J. Wang, B. Zhang, L. Xin, S. Niu, Y. Zhao, M. Xu, X. Chu, D. Zhang, C. Qu, F. Z. Zhao, *Opt. Lett.* **2019**, *44*, 1908.

[23] H. Wang, Y. Wu, M. Ma, S. Dong, Q. Li, J. Du, H. Zhang, Q. Xu, *ACS Appl. Energy Mater.* **2019**, *2*, 2305.

[24] Y. El Ajjouri, F. Palazon, M. Sessolo, H. J. Bolink, *Chem. Mater.* **2018**, *30*, 7423.

[25] M. J. Crane, D. M. Kroupa, J. Y. Roh, R. T. Anderson, M. D. Smith, D. R. Gamelin, *ACS Appl. Energy Mater.* **2019**, *2*, 4560.

[26] F. Palazon, Y. El Ajjouri, H. J. Bolink, *Adv. Energy Mater.* **2020**, *10*, 1902499.

[27] B. Yang, W. Pan, H. Wu, G. Niu, J.-H. Yuan, K.-H. Xue, L. Yin, X. Du, X.-S. Miao, X. Yang, Q. Xie, J. Tang, *Nat. Commun.* **2019**, *10*, 1989.

[28] S. De Wolf, J. Holovsky, S.-J. Moon, P. Löper, B. Niesen, M. Ledinsky, F.-J. Haug, J.-H. Yum, C. Ballif, *J. Phys. Chem. Lett.* **2014**, *5*, 1035.

[29] D. E. McCumber, *Phys. Rev.* **1964**, *136*, A954.

[30] M. Ledinsky, T. Schönfeldová, J. Holovský, E. Aydin, Z. Hájková, L. Landová, N. Neyková, A. Fejfar, S. De Wolf, *J. Phys. Chem. Lett.* **2019**, *10*, 1368.

**2000162** (5 of 5)